Crystal structure and magnetic properties of some new hexagonal ferrites (Ba2Sn2MeFe10-xGaxO22) with the QS-structure

Cadée, M.C.; Groot, H.J.M. de; Jongh, L.J. de; IJdo, D.J.W.

Journal of Magnetism and Magnetic Materials 62 (1986) 367–380
North-Holland, Amsterdam

CRYSTAL STRUCTURE AND MAGNETIC PROPERTIES OF SOME NEW HEXAGONAL FERRITES ($Ba_2Sn_2MeFe_{10-x}Ga_xO_{22}$) WITH THE QS-STRUCTURE

M.C. CADÉE, H.J.M. de GROOT *, L.J. de JONGH * and D.J.W. IJDO

Section of Solid State Chemistry, Department of Chemistry, Gorlaeus Laboratories, P.O. Box 9502, 2300 RA Leiden, The Netherlands

* *Kamerlingh Onnes Laboratory, State University Leiden, P.O. Box 9506, 2300 RA Leiden, The Netherlands*

Received 28 March 1986

The crystal and magnetic structure of the compounds $Ba_2Sn_2MnFe_{10}O_{22}$, $Ba_2Sn_2MnGa_2Fe_8O_{22}$, $Ba_2Sn_2NiFe_{10}O_{22}$ and $Ba_2Sn_2CoFe_{10}O_{22}$ have been determined using neutron powdered diffraction and the Rietveld profile refinement. The neutron diffraction data have been collected at 4.2, 300 K and a temperature above the magnetic transition point T_c. The crystal structures are all of the QS-type, which means they consist of a spinel-block alternated with a so called Q-block. The magnetic structure of these compounds is directly related to the crystallographic structure. In the spinel-block the magnetic moments at the octahedral sites are opposite to the moments at the tetrahedral sites, resulting in a net magnetic moment of the spinel-block. These net moments are antiferromagnetically coupled by superexchange in the Q-block, so that a so called antiferrimagnet is obtained. All magnetic moments are perpendicular to the *c*-axis.

The Mössbauer spectrum of $Ba_2Sn_2ZnGa_2Fe_8O_{22}$ at 300 K (above T_c) could be fitted with three paramagnetic doublets. A correlation of the crystallographic sites and the observed doublets was made by a calculation of the lattice effects to the quadrupole splitting. The distribution of Fe over the sites found in this way is in good agreement with the results obtained from the neutron diffraction data.

The magnetic measurements showed a first saturation at about 100 kOe, corresponding to the alignment to the applied field of the antiferromagnetically coupled net-moments of the spinel-blocks. The second saturation could not be achieved with the available field, but would correspond with the alignment of the individual moments of each site to the applied field. The susceptibility at low fields is high and can be influenced by substitution of Ga or Zn. The compounds showed almost no remanent magnetism.

1. Introduction

In the course of investigations in the $BaO–SnO_2–Fe_2O_3$ system at 1470 K, a compound with composition $BaSn_{0.9}Fe_{5.47}O_{11}$ was found to exist [1]. This hexagonal compound has a hcc-stacked structure, that can be thought to consist of a Q-block and a spinel-block [2], so the notation for this hexagonal ferrite becomes QS.

The Q-block consists of two c-stacked BaO_3-layers, bound by two h-stacked O_4-layers. Between the BaO_3 layers are no cations, between the BaO_3- and O_4-layer one octahedral and one tetrahedral site is occupied. On the boundary with the spinel-block three octahedral sites are occupied.

A considerable number of compounds isostructural to the QS-structure have been reported [2], with general formula $Ba_2Sn_2MeFe_{10}O_{22}$, with Me being a divalent ion that can occupy tetrahedral or octahedral sites in oxyde-structures. A partly substitution of Fe by Ga was reported also.

This new family of hexagonal ferrites possesses interesting magnetic properties, of which some have been reported [2]. In this paper the crystal and magnetic structure of some compounds of this family are reported and it is tried to explain the magnetic properties in relation to the magnetic structure.

2. Experimental

The investigated compounds were prepared by mixing in an agate mortar the appropriate ratios of $BaCO_3$, SnO_2 and Fe_2O_3 and a compound containing the Me^{2+}. The mixture was heated at

1470 K for several days with repeated grindings. Mn was introduced as MnO_2, which decomposes at 1050 K, Ni, Zn and Cd were introduced as the mono-oxides and Co and Mg as the carbonates. In the latter case the mixture was preheated at 600 K in order to decompose the carbonates. Ga was introduced as β-Ga_2O_3.

The reaction mixtures were examined using X-ray diffraction. X-ray powder diffraction patterns were obtained with a Philips PW 1050 diffractometer using CuKα radiation and a graphite monochromator. After a heating time of 7 d, the mixtures consisted of one compound with unit-cell dimensions consistent with the QS-structure. All reaction mixtures were air-quenched from 1470 K. The unit-cell dimensions at room temperature have been collected at 4.2, 300 K and a temperature above the magnetic transition point T_c, using the powder diffractometer at the Petten High Flux Reactor (The Netherlands). A wavelength of about 2.591 Å from the (111) plane of a copper monochromator was used with 30° collimation. The angular range $5.4° < 2\theta < 156.6°$ was scanned in steps of 0.144°. The collected data were corrected for absorption, the maximum absorption correction never exceeded 3.0%. The μR's [3] are listed in table 1. The background points were estimated at regions of the diffraction pattern where reflections were known to be absent. Correction for a possible preferred orientation of the (001) plane was made in the refinement computer program for the Rietveld analysis [4]. The use of glue was rejected because of the higher background it causes in the diffraction pattern.

The Mössbauer experiments were performed in a standard setup constructed at the Kamerlingh Onnes Laboratory [5]. The ^{57}Fe source was embedded in rhodium (isomer shift (IS) = +0.1209 mm/s relative to α-Fe). The velocity calibration was done with a He–Ne laser interferometer.

In order to detect the magnetic transition points magnetic susceptibility measurements were carried out above 80 K with a Faraday balance equipped with a temperature controller [6]. Magnetization measurements at 4.2 K for fields up to 56 kOe were performed by means of a P.A.R. vibrating sample magnetometer [7]. Magnetization experiments in very high fields up to 400 kOe were done in the pulsed-field magnet of the Kamerlingh Onnes Laboratory. In this apparatus the field-variation in time behaves like $H(t) = H_{max} \sin \omega t$ with $\omega = 210$ rad/s and half a period is used. An extensive description of this equipment is given elsewhere [8].

3. Determination of the structures

The crystal and magnetic structures of four compounds, $Ba_2Sn_2MnFe_{10}O_{22}$, $Ba_2Sn_2NiFe_{10}O_{22}$, $Ba_2Sn_2CoFe_{10}O_{22}$ and $Ba_2Sn_2MnGa_2Fe_8O_{22}$ have been determined. The procedure used was the following. First the neutron diffraction pattern collected above T_c was refined. The atomic param-

Table 1
Diffraction data and refinement results for the investigated compounds of the QS-structure

Compound	Temp. (K)	λ (Å)	μR	a-axis (Å)	c-axis (Å)	B	R_I	R_N	R_M	R_p	R_{wp}	R_{exp}
$Ba_2Sn_2MnFe_{10}O_{22}$	573	2.5912 (4)	0.16	5.9596 (1)	14.3921 (5)	0.70 (4)	2.71	2.71	–	5.18	6.07	2.71
$Ba_2Sn_2MnFe_{10}O_{22}$	300	2.5923 (3)	0.17	5.9441 (1)	28.6809 (10)	0.39 (4)	2.27	2.00	5.65	5.06	6.03	2.38
$Ba_2Sn_2MnFe_{10}O_{22}$	4.2	2.5923 (3)	0.17	5.9360 (1)	28.6245 (10)	−0.04 (4)	2.59	2.19	4.20	5.156	5.79	2.17
$Ba_2Sn_2MnGa_2Fe_8O_{22}$	300	2.5907 (3)	0.21	5.9331 (1)	14.3617 (4)	0.42 (3)	2.38	2.38	–	5.19	6.35	2.11
$Ba_2Sn_2MnGa_2Fe_8O_{22}$	4.2	2.5906 (3)	0.22	5.9124 (1)	28.6112 (10)	−0.33 (4)	4.36	3.74	8.32	6.87	7.81	3.16
$Ba_2Sn_2NiFe_{10}O_{22}$	600	2.5921 (3)	0.21	5.9365 (1)	14.3549 (4)	0.66 (3)	1.74	1.74	–	3.94	4.50	2.20
$Ba_2Sn_2NiFe_{10}O_{22}$	300	2.5921 (3)	0.20	5.9218 (1)	28.6128 (8)	0.36 (3)	1.73	1.14	7.10	4.20	4.94	2.31
$Ba_2Sn_2NiFe_{10}O_{22}$	4.2	2.5906 (3)	0.20	5.9161 (1)	28.5665 (13)	−0.01 (5)	2.68	1.69	7.00	6.63	7.76	2.44
$Ba_2Sn_2CoFe_{10}O_{22}$	500	2.5906 (3)	0.34	5.9405 (1)	14.3581 (5)	0.54 (3)	2.05	2.05	–	4.78	5.17	2.50
$Ba_2Sn_2CoFe_{10}O_{22}$	300	2.5906 (3)	0.32	5.9304 (1)	28.6466 (10)	0.47 (3)	3.04	2.57	9.42	5.13	5.72	2.41
$Ba_2Sn_2CoFe_{10}O_{22}$	4.2	2.5906 (3)	0.32	5.9234 (1)	28.5962 (13)	−0.01 (4)	3.63	2.97	6.58	6.22	6.91	2.67

Table 2
Atomic parameters of $Ba_2Sn_2MnFe_{10}O_{22}$ at 573 K (spacegroup $P\bar{3}m$), $y = 2x$

Atom	Position	x	z	Occupation rate (%)
Ba	2d	0.3333	0.4294 (9)	100
Mn				46.4 (4)
Tetr(1)	2d	0.3333	0.9567 (19)	
Fe				53.6 (4)
Fe Tetr(2)	2c	0.0	0.3757 (5)	100
Sn				85 (2)
Oc(1)	2d	0.3333	0.6789 (10)	
Fe				15 (2)
Mn				7.2 (4)
Oc(2)	1a	0.0	0.0	
Fe				92.8 (4)
Sn				5 (1)
Oc(3)	6i	0.1695 (4)	0.1744 (3)	
Fe				95 (1)
O(1)	2c	0.0	0.2418 (8)	100
O(2)	2d	0.3333	0.0904 (7)	100
O(3)	6i	0.1517 (5)	0.9125 (4)	100
O(4)	6i	0.5048 (11)	0.2435 (4)	100
O(5)	6i	0.1771 (6)	0.5919 (4)	100

eters of $BaSn_{0.9}Fe_{5.47}O_{11}$ [2] were used as starting parameters. The variables in the first stage of the Rietveld profile refinement [4] were: a scale factor, three half-width parameters defining the Gaussian lineshape, the counter zero error, the unit-cell dimensions and an overall temperature factor.

After the first runs, the atomic parameters, a preferred orientation parameter for the (001) planes and an asymmetry parameter below $2\theta = 40°$ were introduced. Next the occupation rates of Sn, Fe and the divalent ion at the octahedral and tetrahedral sites were also variable within the overall formula and with the limitation that the total occupation rate of a site remained 100%. In the case of $Ba_2Sn_2MnGa_2Fe_8O_{22}$ the occupation rate of Ga was variable over the octahedral and tetrahedral sites also, with the same restrictions. Only an overall temperature factor was calculated, because individual temperature factors and occupation rates have a high correlation in the computer program. The coherent scattering lengths assumed are: Ba 5.25, Sn 6.228, Fe 9.54, 0 5.805, Mn −3.73, Ga 7.29, Ni 10.3, Co 2.53 fm [9]. The calculated R-factors in the nuclear refinements were R_I, R_p, R_{wp} and $R_{expected}$, for the refinement of the magnetic structure $R_{magnetic}$ was calculated also. For the definition of the R-factors see ref. [10]. The obtained occupation rates in the refinements of diffraction data above T_c were used in the refinements of the magnetic structure as constants. A (110) section of the crystal structure is shown in fig. 2a, with an indication of the different sites.

As reported [2], the magnetic structure has a c-axis of twice the c-axis of the crystal structure and the same a-axis. The spin-arrangement for the magnetic structure was derived from the magnetic structures of $BaFe_{12}O_{19}$ (M) and $Ba_2Zn_2Fe_{12}O_{22}$ (Zn2Y) [11,12]. This model has much in common with the proposed magnetic structure of $KFe_{11}O_{17}$

Table 3
Atomic parameters and magnetic moments in the magnetic structure $Ba_2Sn_2MnFe_{10}O_{22}$ at 4.2 and 300 K, $y = 2x$

Atom	Position	x (4.2 K)	x (300 K)	z (4.2 K)	z (300 K)	M_x (4.2 K)	M_x (300 K)
Ba	2d	0.3333	0.3333	0.2156 (4)	0.2131 (4)	–	–
Tetr(1)	2d	0.3333	0.3333	0.4758 (4)	0.4763 (5)	4.38 (8)	3.45 (10)
Tetr(2)	2c	0.0	0.0	0.1883 (2)	0.1881 (2)	−4.16 (6)	−1.47 (7)
Oc(1)	2d	0.3333	0.3333	0.3378 (4)	0.3391 (4)	0.51 (6)	0.28 (7)
Oc(2)	1a	0.0	0.0	0.0	0.0	3.68 (8)	2.63 (11)
Oc(3)	6i	0.1700 (3)	0.1698 (3)	0.0875 (1)	0.0873 (1)	4.16 (4)	1.97 (5)
O(1)	2c	0.0	0.0	0.1221 (4)	0.1208 (3)	–	–
O(2)	2d	0.3333	0.3333	0.0448 (3)	0.0452 (3)	–	–
O(3)	6i	0.1502 (5)	0.1512 (4)	0.4571 (2)	0.4568 (2)	–	–
O(4)	6i	0.5027 (14)	0.5026 (13)	0.1215 (2)	0.1213 (2)	–	–
O(5)	6i	0.1743 (5)	0.1757 (5)	0.2956 (2)	0.2956 (2)	–	–

Table 4
Atomic parameters of $Ba_2Sn_2CoFe_{10}O_{22}$ at 500 K (spacegroup $P\bar{3}m$), $y = 2x$

Atom	Position	x	z	Occupation rate (%)
Ba	2d	0.3333	0.4253 (8)	100
Co				26.6 (9)
Tetr(1)	2d	0.3333	0.9560 (6)	
Fe				74.4 (9)
Fe Tetr(2)	2c	0.0	0.3756 (5)	100
Sn				85.3 (21)
Co Oc(1)	2d	0.3333	0.6805 (8)	5.0 (3)
Fe				9.7 (21)
Co				7.0 (7)
Oc(2)	1a	0.0	0.0	
Fe				93.0 (47)
Sn				4.9 (7)
Co Oc(3)	6i	0.1702 (4)	0.1728 (3)	5.0 (3)
Fe				90.1 (8)
O(1)	2c	0.0	0.2389 (9)	100
O(2)	2d	0.3333	0.0882 (7)	100
O(3)	6i	0.1551 (5)	0.9150 (4)	100
O(4)	6i	0.4939 (11)	0.2462 (6)	100
O(5)	6i	0.1734 (5)	0.5918 (4)	100

[13,14], described as an antiferrimagnetic compound.

The model used for the refinements has the magnetic moments of the atoms at the tetrahedral sites in a direction opposite to the moments of the octahedral sites. At the two BaO_3-layers, the moments of the bounding tetrahedral sites (Tetr(2)) are coupled antiferromagnetically, in a way already suggested [2] and reported for the magnetic structure of $BaCaFe_4O_8$ [15]. In the spinel-block and the bounding O_4-layer of the Q-block there are 4 tetrahedral sites occupied and 9 octahedral sites, two of the octahedral sites are occupied by Sn, but nevertheless there are always more magnetic moments at the octahedral sites, resulting in a net magnetic moment for the block between the BaO_3-layers. The net magnetic moment of the bounding block is opposite, because of the antiferromagnetic coupling of the Tetr(2) sites, thus an antiferrimagnet [13] is obtained.

Only in a direction perpendicular to the z-axis a magnetic moment was found. The magnetic form-factors were taken from ref. [16]. The results of the refinements are reported in tables 2 to 9. The magnetic moments of the sites are listed for an occupation rate of 100%. This is because some sites are occupied by both magnetic and nonmagnetic atoms. With the occupation rates refined from the neutron diffraction data collected above T_c, the moments of the magnetic atoms can be easily calculated. The magnetic R-factors are listed in table 1, figs. 1a, b, c show the agreement between observed and calculated profiles of $Ba_2Sn_2MnFe_{10}O_{22}$ at 575, 4.2 and 300 K, respectively. These are given as an example for the other refinements reported in this paper. A (110) section of the magnetic structure of $Ba_2Sn_2MnFe_{10}O_{22}$ is presented in fig. 2b. In table 10 the relevant distances of the structure of $Ba_2Sn_2MnFe_{10}O_{22}$ at 573 K are listed and in table 11 the relevant angles of this structure.

Table 5
Atomic parameters and magnetic moments in the magnetic structure of $Ba_2Sn_2CoFe_{10}O_{22}$ at 4.2 K and 300 K, $y = 2x$

Atom	Position	x (4.2 K)	x (300 K)	z (4.2 K)	z (300 K)	M_x (4.2 K)	M_x (300 K)
Ba	2d	0.3333	0.3333	0.2114 (5)	0.2126 (4)	–	–
Tetr(1)	2d	0.3333	0.3333	0.4768 (3)	0.4774 (3)	3.96 (12)	2.40 (10)
Tetr(2)	2c	0.0	0.0	0.1877 (3)	0.1879 (2)	−3.77 (7)	−1.35 (6)
Oc(1)	2d	0.3333	0.3333	0.3379 (5)	0.3405 (3)	0.08 (6)	0.05 (6)
Oc(2)	1a	0.0	0.0	0.0	0.0	4.10 (10)	3.65 (10)
Oc(3)	6i	0.1707 (3)	0.1707 (3)	0.0866 (1)	0.0865 (1)	3.99 (5)	2.45 (5)
O(1)	2c	0.0	0.0	0.1209 (5)	0.1210 (4)	–	–
O(2)	2d	0.3333	0.3333	0.0436 (4)	0.0445 (3)	–	–
O(3)	6i	0.1552 (6)	0.1547 (4)	0.4581 (2)	0.4576 (2)	–	–
O(4)	6i	0.4971 (15)	0.4937 (8)	0.1224 (3)	0.1224 (2)	–	–
O(5)	6i	0.1725 (5)	0.1735 (4)	0.2959 (3)	0.2957 (2)	–	–

Table 6
Atomic parameters of $Ba_2Sn_2NiFe_{10}O_{22}$ at 600 K (space group $P\bar{3}m$), $y = 2x$

Atom	Position	x	z	Occupation rate (%)
Ba	2d	0.3333	0.4235 (7)	100
Fe Tetr(1)	2d	0.3333	0.9547 (4)	100
Fe Tetr(2)	2c	0.0	0.3743 (4)	100
Sn				86.9 (18)
Oc(1)	2d	0.3333	0.6789 (7)	
Fe				13.1 (18)
Ni Oc(2)	1a	0.0	0.0	100
Sn				4.7 (6)
Oc(3)	6i	0.1696 (3)	0.1725 (2)	
Fe				95.3 (6)
O(1)	2c	0.0	0.2393 (8)	100
O(2)	2d	0.3333	0.0890(6)	100
O(3)	6i	0.1572 (4)	0.9145 (3)	100
O(4)	6i	0.4956 (9)	0.2449 (5)	100
O(5)	6i	0.1752 (4)	0.5912 (3)	100

Table 8
Atomic parameters of $Ba_2Sn_2MnGa_2Fe_8O_{22}$ at 300 K (space group $P\bar{3}m$), $y = 2x$

Atom	Position	x	z	Occupation rate (%)
Ba	2d	0.3333	0.4266 (7)	100
Mn				48.2 (3)
Tetr(1)	2d	0.3333	0.9517 (12)	
Fe				51.8 (3)
Fe				60.5 (3)
Tetr(2)	2c	0.0	0.3765 (5)	
Ga				39.5 (3)
Sn Oc(1)	2d	0.3333	0.6781 (8)	100
Fe				96.3 (6)
Oc(2)	1a	0.0	0.0	
Mn				3.7 (6)
Fe				80.2 (9)
Oc(3)	6i	0.1692 (3)	0.1738 (2)	
Ga				19.8 (9)
O(1)	2c	0.0	0.2407 (7)	100
O(2)	2d	0.3333	0.0942 (69	100
O(3)	6i	0.1506 (4)	0.9134 (3)	100
O(4)	6i	0.4955 (10)	0.2434 (4)	100
O(5)	6i	0.1743 (4)	0.5912 (3)	100

4. Structural results

The obtained crystal structures are all of the QS-type, as to be expected from the X-ray powder diffraction patterns. Of particular interest is the distribution of the divalent cations over the available tetrahedral and octahedral sites.

In $Ba_2Sn_2MnFe_{10}O_{22}$ almost all Mn-atoms are found at the Tetr(1) site, which is usual for Mn^{2+} in related oxide-structures. No Mn was found at the Tetr(2) site, whereas a low occupation rate of Mn at this place can be easily detected because of the large difference in the coherent scattering lengths. The charge-compensation of the O-atoms has improved except for O(1), compared to $BaSn_{0.9}Fe_{5.47}O_{11}$ (see table 12). The higher charge-compensation of O(1) is due to the higher charge on Oc(3).

In $Ba_2Sn_2MnGa_2Fe_8O_{22}$ the Ga-atoms have

Table 7
Atomic parameters and magnetic moments in the magnetic structure of $Ba_2Sn_2NiFe_{10}O_{22}$ at 4.2 and 300 K, $y = 2x$

Atom	Position	x (4.2 K)	x (300 K)	z (4.2 K)	z (300 K)	M_x (4.2 K)	M_x (300 K)
Ba	2d	0.3333	0.3333	0.2110 (6)	0.2116 (3)	–	–
Tetr(1)	2d	0.3333	0.3333	0.4769 (3)	0.4775 (2)	4.09 (10)	2.68 (4)
Tetr(2)	2c	0.0	0.0	0.1881 (3)	0.1880 (2)	−4.19 (8)	−2.63 (4)
Oc(1)	2d	0.3333	0.3333	0.3385 (5)	0.3401 (3)	0.27 (7)	0.35 (6)
Oc(2)	1a	0.0	0.0	0.0	0.0	3.23 (10)	2.90 (7)
Oc(3)	6i	0.1702 (5)	0.1697 (3)	0.0864 (2)	0.0862 (1)	3.85 (5)	2.43 (4)
O(1)	2c	0.0	0.0	0.1221 (6)	0.1203 (4)	–	–
O(2)	2d	0.3333	0.3333	0.0437 (4)	0.0439 (3)	–	–
O(3)	6i	0.1570 (7)	0.1569 (4)	0.4583 (3)	0.4580 (2)	–	–
O(4)	6i	0.4966 (14)	0.4962 (9)	0.1220 (4)	0.1223 (2)	–	–
O(5)	6i	0.1732 (7)	0.1740 (4)	0.2957 (3)	0.2959 (2)	–	–

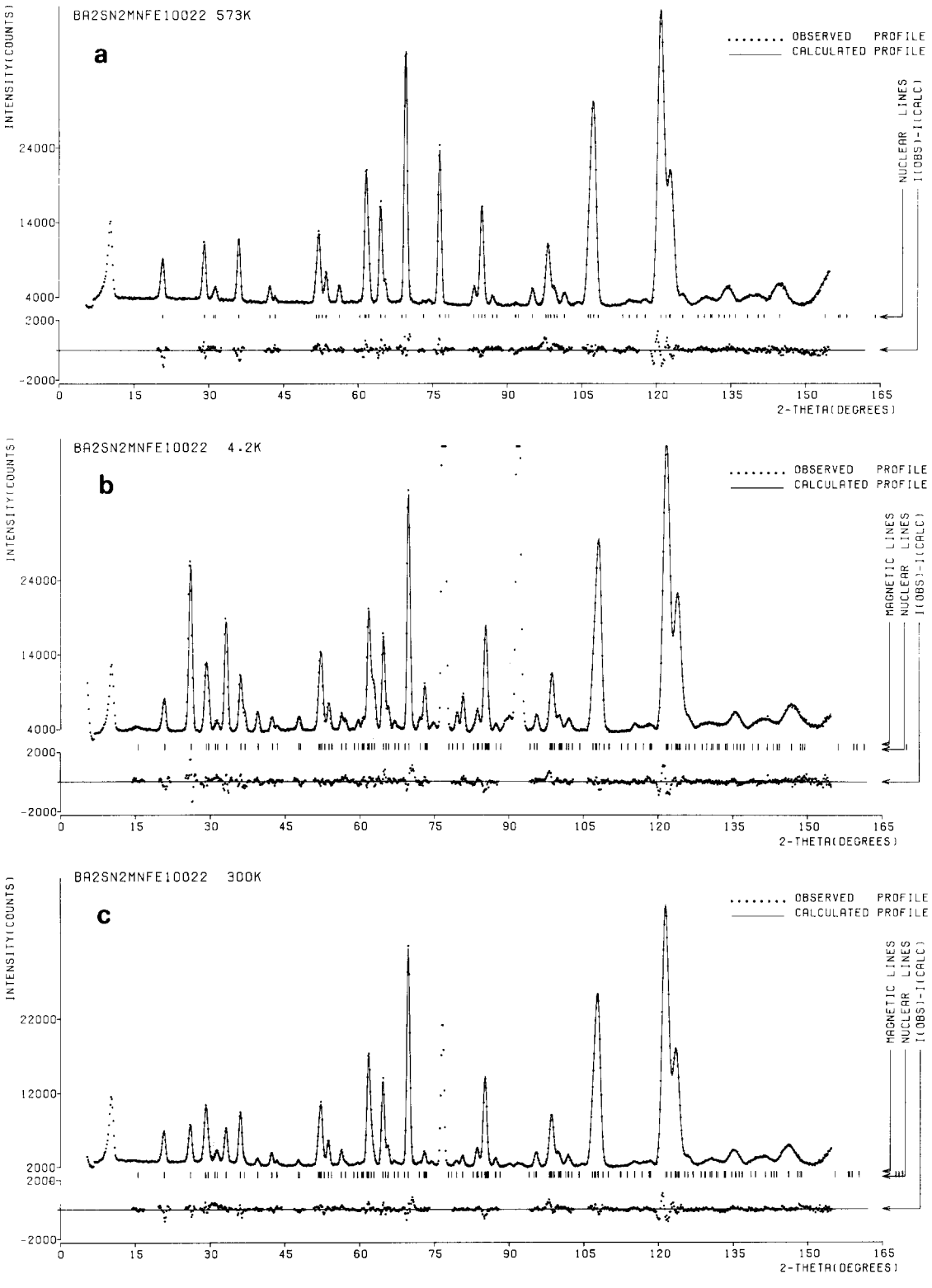

Fig. 1. (a) Neutron diffraction profile of $Ba_2Sn_2MnFe_{10}O_{22}$ at 573 K; (b) neutron diffraction profile of $Ba_2Sn_2MnFe_{10}O_{22}$ at 4.2 K; (c) neutron diffraction profile of $Ba_2Sn_2MnFe_{10}O_{22}$ at 300 K. Observed profiles (dots) and calculated profiles (full line). A difference curve (observed-calculated) appears at the bottom of the figure. Thick marks below the profiles indicate the Bragg reflections included in the calculation.

Table 9
Atomic parameters and the magnetic moment of the site of $Ba_2Sn_2MnGa_2Fe_8O_{22}$ at 4.2 K in the magnetic unit cell, $y = 2x$

Atom	Position	x	z	$M(\mu_B)$
Ba	2d	0.3333	0.2128 (3)	–
Tetr(1)	2d	0.3333	0.4773 (4)	3.97 (9)
Tetr(2)	2c	0.0	0.1889 (3)	−2.27 (7)
Oc(1)	2d	0.3333	0.3394 (3)	–
Oc(2)	1a	0.0	0.0	2.62 (9)
Oc(3)	6i	0.1700 (3)	0.0864 (1)	3.28 (4)
O(1)	2c	0.0	0.1217 (4)	–
O(2)	2d	0.3333	0.0467 (3)	–
O(3)	6i	0.1516 (5)	0.4573 (2)	–
O(4)	6i	0.4980 (14)	0.1217 (2)	–
O(5)	6i	0.1728 (5)	0.2969 (2)	–

some influence on the distribution of Sn over the octahedral sites. However, it must be kept in mind that in this compound the distribution of Sn, Ga and Fe over the octahedral sites is difficult to determine, because of the relatively low differences in the coherent scattering lengths. Of further importance is the observation that Ga substitutes Fe at the Tetr(2) site, because the magnetic moments of this site are coupled antiferromagnetically, and are responsible for the antiferromagnetic coupling of the net-moments of the magnetic blocks. So Ga-substitution influences the

Table 11
Relevant angles (degrees) in the structure of $Ba_2Sn_2MnFe_{10}O_{22}$ at 573 K

O(2)–Tetr(1)–O(3)	108.7 (6) 3×
O(3)–Tetr(1)–O(3)	110.2 (5) 3×
O(1)–Tetr(2)–O(5)	104.3 (3) 3×
O(5)–Tetr(2)–O(5)	114.1 (2) 3×
O(4)–Oc(1)–O(4)	92.1 (6) 3×
O(4)–Oc(1)–O(5)	90.7 (3) 6×
O(4)–Oc(1)–O(5)	175.9 (7) 3×
O(5)–Oc(1)–O(5)	86.3 (5) 3×
O(3)–Oc(2)–O(3)	84.9 (2) 6×
O(3)–Oc(2)–O(3)	180.0 (0) 3×
O(1)–Oc(3)–O(2)	173.5 (4) 1×
O(1)–Oc(3)–O(3)	83.4 (3) 2×
O(1)–Oc(3)–O(4)	96.4 (4) 2×
O(2)–Oc(3)–O(3)	91.7 (3) 2×
O(2)–Oc(3)–O(4)	87.8 (3) 2×
O(3)–Oc(3)–O(3)	81.3 (3) 1×
O(3)–Oc(3)–O(4)	89.2 (3) 2×
O(3)–Oc(3)–O(4)	170.5 (4) 2×
O(4)–Oc(3)–O(4)	100.3 (6) 1×

Table 10
Relevant distances (Å) in the structure of $Ba_2Sn_2MnFe_{10}O_{22}$ at 573 K

Attractive		Repulsive (below 3 Å)	
Ba–O(4)	3.21 (1) 3×	Oc(3)–Oc(3)	2.93 (1) 3×
Ba–O(5)	2.84 (1) 3×	O(1)–O(3)	2.72 (1) 3×
Ba–O(5)	3.00 (1) 6×	O(1)–O(4)	2.98 (1) 6×
Tetr(1)–O(2)	1.92 (2) 1×	O(2)–O(3)	2.98 (1) 6×
Tetr(1)–O(3)	1.98 (1) 3×	O(2)–O(4)	2.83 (1) 3×
Tetr(2)–O(1)	1.93 (1) 1×	O(3)–O(3)	2.71 (1) 2×
Tetr(2)–O(5)	1.89 (1) 3×	O(3)–O(4)	2.87 (1) 2×
Oc(1)–O(4)	2.01 (1) 3×	O(4)–O(4)	2.98 (2) 2×
Oc(1)–O(5)	2.04 (1) 3×	O(4)–O(5)	2.88 (1) 2×
Oc(2)–O(3)	2.01 (1) 6×	O(5)–O(5)	2.79 (1) 2×
Oc(3)–O(1)	2.00 (1) 1×		
Oc(3)–O(2)	2.08 (1) 1×		
Oc(3)–O(3)	2.08 (1) 2×		
Oc(3)–O(4)	2.00 (1) 2×		

magnetic properties of this compounds (see below) and the lowering of T_c in the Ga-substituted compounds can be explained in this way.

In $Ba_2Sn_2NiFe_{10}O_{22}$ all Ni was found at the Oc(2) position, thus lowering the charge-compensation of O(3). The occupation rates of Tetr(2) remains 100% Fe, resulting in a high T_c of this compound (see table 13).

In $Ba_2SnCoFe_{10}O_{22}$ Co is distributed over tetrahedral and octahedral sites. Here again the distribution over the sites is less certain because of the low differences in the coherent scattering lengths. All compounds with a M^{2+} ion have a more regular charge-compensation then $BaSn_{0.9}Fe_{5.47}O_{11}$.

The obtained magnetic structures all show the proposed model (fig. 2b), with the moments of the tetrahedral sites opposite the moments of the octahedral sites. The net-magnetic moments of the blocks are influenced by the distribution of the

Table 12
Charge compensations of oxygen atoms in the investigated compounds with the QS-structure

Compound	O(1)	O(2)	O(3)	O(4)	O(5)
$BaSn_{0.9}Fe_{5.47}O_{11}$	2.19	2.19	2.29	1.73	1.86
$Ba_2Sn_2MnFe_{10}O_{22}$	2.27	2.16	2.14	1.83	1.89
$Ba_2Sn_2MnGa_2Fe_8O_{22}$	2.25	2.13	2.11	1.83	1.92
$Ba_2Sn_2NiFe_{10}O_{22}$	2.27	2.27	2.10	1.83	1.90
$Ba_2Sn_2CoFe_{10}O_{22}$	2.25	2.19	2.18	1.80	1.88

magnetic ions over the sites. The net-moments of the blocks are calculated using the observed occupation rates and the refined moments, and also using the spin-only value of the different ions. These results are presented in table 13, where also the experimental moments, obtained from the pulsed field measurements are listed. The T_c's which have been given in ref. [2] are included in this table.

The net-moment obtained by using the found occupation rates and the theoretical spin-only values show the best agreement with the experimentally obtained moments. The moments calculated with the refined moments from the neutron diffraction experiments are always considerable lower than the moments obtained from the magnetization measurements at 4.2 K. This is not unusual, and is also found in several other investigations [15,19,20].

5. Results of the Mössbauer experiments

In fig. 3 the Mössbauer spectrum of $Ba_2Sn_2ZnGa_2Fe_8O_{22}$ is shown. The spectrum was analyzed in terms of three doublets named α, β and γ. The parameters are listed in table 14. Here IS is the isomer-shift relative to rhodium, Δ the quadrupole splitting and Int the relative weight of the doublet in the spectrum. The spectrum was fitted with Lorentzian lines and the results, to-

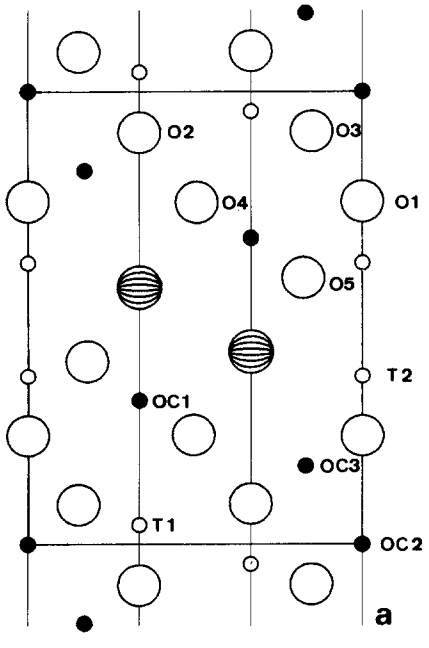

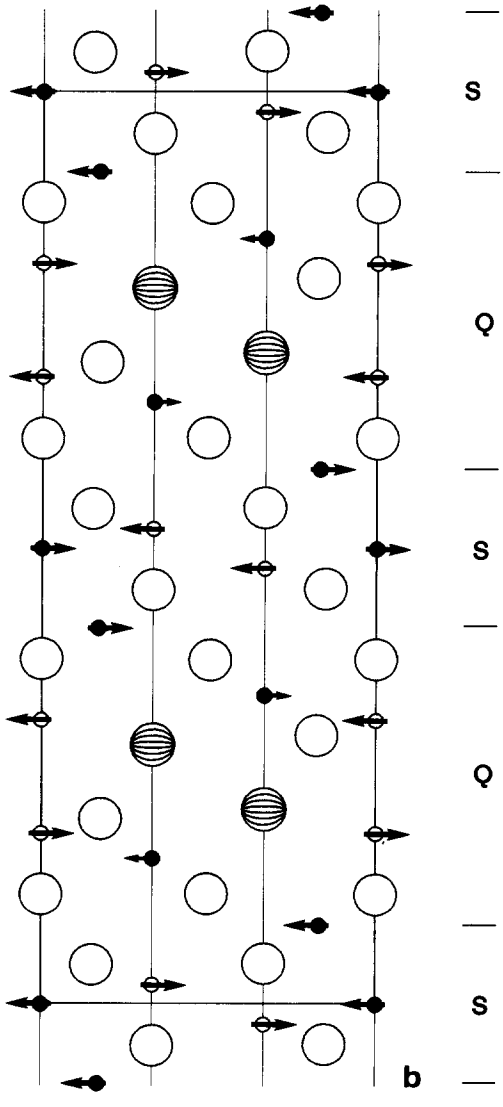

Fig. 2. (a) (110) plane of the structure of $Ba_2Sn_2MnFe_{10}O_{22}$, Shaded circles: Ba; open circles: O; small open circles: filled tetrahedral sites; solid circles: filled octahedral sites. The name of the different positions is indicated; (b) (110) plane of the magnetic structure of $Ba_2Sn_2MnFe_{10}O_{22}$. The Q- and S-blocks are indicated. The moment of Oc(1) has been drawn with a little arrow because Oc(1) is preferently occupied by Sn.

Table 13
Refined (from neutron diffraction data), observed (from magnetization measurements) and calculated (from the magnetic structure model using spin-only values) moments in μ_B of several compounds of the QS-structure. The distribution of M^{2+} over tetrahedral and octahedral sites is given as result of the neutron diffraction experiments or otherwise as the distribution necessary to fit the calculated and observed moments of the compounds. Cd^{2+} and Zn^{2+} are supposed to occupy tetrahedral sites only

Compound	Moment refined 4.2 K	Moment refined 300 K	Moment obs. 4.2 K	Moment obs. 77 K	Moment obs. 300 K	Spin only value M^{2+}	M^{2+} tetr. (%)	M^{2+} oct. (%)	Moment calc.	T_c (K)
$Ba_2Sn_2MnFe_{10}O_{22}$	12.6 (3)	5.4 (3)	15.2 (3)	14.4 (3)	8.1 (4)	5	100	0	15.0	380
$Ba_2Sn_2MnGa_2Fe_8O_{22}$	9.8 (3)	–	14.9 (3)	–	–	5	100	0	13.1	–
$Ba_2Sn_2NiFe_{10}O_{22}$	10.3 (4)	8.2 (3)	13.2 (3)	–	–	2	0	100	12.0	444
$Ba_2Sn_2CoFe_{10}O_{22}$	12.7 (4)	9.5 (4)	17.6 (3)	–	–	3	53	47	15.1	378
$Ba_2Sn_2ZnFe_{10}O_{22}$	–	–	14.6 (4)	–	–	0	100	0	20.0	–
$Ba_2Sn_2CuFe_{10}O_{22}$	–	–	13.7 (3)	12.6 (4)	6.5 (5)	1	35	65	13.7	375
$Ba_2Sn_2MgFe_{10}O_{22}$	–	–	13.0 (3)	–	–	0	30	70	13.0	334
$Ba_2Sn_2CdFe_{10}O_{22}$	–	–	14.2 (3)	12.7 (4)	5.2 (5)	0	100	0	20.0	–
$(BaSn_{09}Fe_{5.47}O_{11})_2$	–	–	14.8 (3)	14.3 (3)	8.9 (4)	–	–	–	14.8	420

gether with the separate peaks are represented by the solid curves in fig. 3. To our opinion this reflects the fact that each doublet may correspond to the absorption spectrum of different sites.

The main part of the transmission spectrum, represented by the α-doublet, and coming from 57% of the ^{57}Fe nuclei, shows the characteristics of a high-spin Fe^{3+} absorption, whereas the other doublets, in particular the β-doublet, are different. From table 14 may be concluded that the quadrupole splittings are quite large, especially for

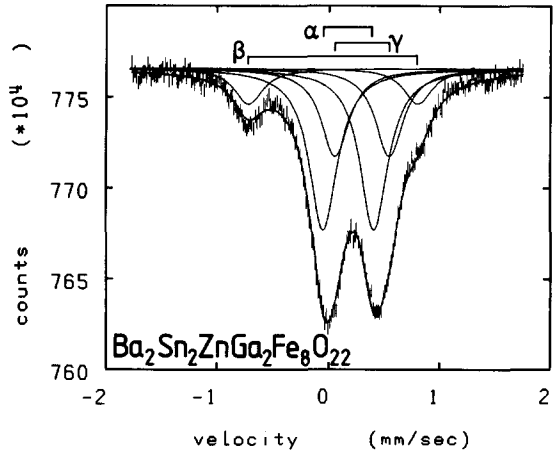

Fig. 3. Observed and fitted Mössbauer spectrum of $Ba_2Sn_2ZnGa_2Fe_8O_{22}$ at 300 K. Also the individual contribution of each doublet is shown.

the β-doublet, where a Δ of 1.52 mm/s is found. Usually, Fe at the tetrahedral site of a spinel-structure does not show quadrupole splitting at all, whereas for the Fe-atoms at the octahedral sites Δ-values less than 0.5 mm/s are reported [21]. Also the values for the IS are rather unusual. Normally high-spin Fe^{3+}-compounds show IS-values in the region $+0.07-+0.41$ mm/s and the value for the IS found for the β-doublet is outside this range (see fig. 4).

In the present case, however, unusual behaviour is expected for two reasons. First the spinel-block is not a perfect spinel structure and especially the Fe-atoms close to the Q-blocks (i.e. Tetr(2) sites) resides in an environment that may cause important field-gradients and thus large Δ-values. Second the charge distribution in the spinel-block is not homogeneous since it is the Zn^{2+} ion at the Tetr(1)-site that compensates for the electron deficit of the S-block as a whole in order to obtain stoichiometry. This may give rise to covalency effects. It is not straightforward to obtain an easy relationship between the charge distribution and the Mössbauer parameters but it is a well-known fact that the IS is directly related to the electron density at the Fe-nucleus and is therefore sensitive to inhomogeneous charge distributions. In order to enlighten these points the lattice contribution to the quadrupole splitting for each site was calculated. In these calculations the structure and oc-

Table 14
Observed isomer shifts relative to Rhodium and observed and calculated quadrupole splittings Δ(mm/s), relative weight of the doublets of the Mössbauer spectrum at 300 K of $Ba_2Sn_2ZnGa_2Fe_8O_{22}$ and comparable neutron diffraction results from $Ba_2Sn_2MnGa_2Fe_8O_{22}$

Doublet	IS (mm/s)	Δ (obs.) (mm/s)	Lattice Δ (calc.) (mm/s)	Int (%) (Mössb.)	Int (%) (neutron)	Assigned sites
α	0.184 (2)	0.459 (2)	0.43 (10)	57 (1)	60 (1)	Oc (3)
β	0.047 (1)	1.52 (1)	0.62 (10)	13 (1)	15 (1)	Tetr (2)
γ	0.307 (2)	0.485 (2)	0.21 (10)	30 (1)	25 (1)	Tetr (1) + Oc (2)

cupation rates as determined in the neutron diffraction experiments were used. Furthermore it was assumed that one of the two Tetr(1) sites in each S-block was occupied by Zn^{2+}, and the other thus by Fe^{3+}. This seems reasonable from the point of view of best possible charge compensation. The results of the calculations are given in table 14. Indeed it appears that at the Tetr(2) site the calculated value for Δ is quite large. It appears that the α-doublet originates from the Fe-atoms at the Oc(3) sites, the β-doublet from the Fe-atoms at the Tetr(2) sites and the γ-doublet from the Fe-atoms at the Tetr(1) and Oc(1) sites together.

These assignments may be compared with the results from the neutron diffraction experiments. If the relative occupations by Fe at the different sites are calculated these results must correspond to the intensity ratios found in the analysis of the Mössbauer spectra. The neutron diffraction results of $Ba_2Sn_2MnGa_2Fe_8O_{22}$ are also shown in table 14 and are in good agreement with the Mössbauer findings on $Ba_2Sn_2ZnGa_2Fe_8O_{22}$. These compounds can be compared because Mn^{2+} was found to occupy almost only the Tetr(1) site.

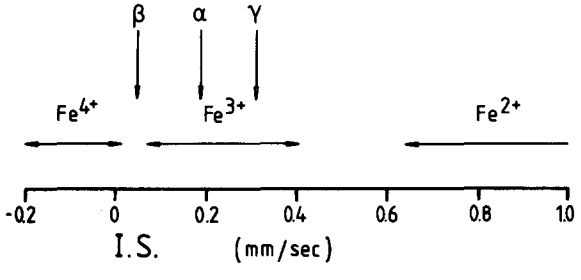

Fig. 4. Distribution of the isomershift (IS) relative to rhodium for compounds with Fe^{2+}, Fe^{3+} and Fe^{4+}. The IS of the observed doublets is indicated in the figure.

As regards the observed values for the IS it appears that it is larger at the Oc(2) and Tetr(1) sites. This may be explained as follows. Since these sites are located close to the Zn-occupied Tetr(1) site the effective valence of the Fe-ions may be somewhat lower than 3 + . The IS values usually observed for Fe^{2+} are in the range +0.62– + 1.43 mm/s so indeed the IS of the γ-doublet is somewhat higher than that of the α-doublet, i.e. shifted towards the range of Fe^{2+} values (see fig. 4). On the other hand, since the total charge balances there must be an electron deficit at the boundary of the Q- and S-block, i.e. at the Tetr(2) site, where the effective valence should be higher that 3 + . This may explain why the observed IS of the β-doublet is close to the region for the values of Fe^{4+} (see fig. 4). It seems as if the effect is even stronger, probably due to the oxygen in the Q-block or the Sn^{4+} at the Oc(2) site.

Since high-spin Fe^{3+} does not carry orbital momentum it is expected that there are no ligand-field effects and the observed quadrupole splittings should be originating from the lattice only. Indeed the observed value is equal to to the calculated lattice Δ for the α-doublet (table 14). However, for the β- and γ-doublet the observed splitting is much larger than the calculated contribution (table 14). These differences are attributed to ligand-field effects since the covalent ions carry orbital moment. Because both ligand-field and the lattice contribution increase with the distortion of the surroundings of the ion, it follows that the site with the highest lattice contribution should show the largest quadrupole splitting anyhow. This supports the assignment of the β-doublet to the Fe at the Tetr(2) sites.

Also a room-temperature spectrum was taken from $Ba_2Sn_2ZnGa_3Fe_7O_{22}$. The spectrum was exactly the same as that shown in fig. 3, which indicates the random distribution of the third Ga^{3+} ion over the different tetrahedral- and octahedral sites, in agreement with the conclusions from the magnetization experiments, discussed below.

No attempt was made to take Mössbauer spectra from any of the compounds that is magnetically ordered at room temperature. Interpretation of such a spectrum would become very difficult, since each of the 4 different sites occupied with Fe may show an 8-line hyperfine split spectrum. Therefore only the paramagnetic phase of $Ba_2Sn_2ZnGa_2Fe_8O_{22}$ was examined.

6. Results of the magnetic measurements

The magnetization curves at 4.2 K all show the same characteristic form (fig. 5). These curves can be divided in two parts, the first corresponding to the high susceptibility range in low fields (up to 50 kOe) and the second to the high field region where the susceptibility is much lower. We attribute the sharp increase of the magnetization in low fields to the interaction of H with the net moment μ of the magnetic blocks. For $H > 100$ kOe all μ's are aligned along the applied field. This first saturation may be achieved in relatively low fields since the superexchange between the S-blocks goes via the Q-blocks and will therefore be small. This also explains the attraction of these compounds by a hand-magnet at room temperature. The high-field part however, corresponds to the interaction of the applied field with the individual (antiferromagnetically coupled) moments in the S-blocks. Complete saturation of these compounds is not easy to obtain, for example, in $Ba_2Sn_2MnFe_{10}O_{22}$ the magnetization at 120 kOe is $15.3\mu_B$, at 400 kOe $16.1\mu_B$ whereas the magnetization at complete saturation would be $55\mu_B$. When this flat part of the magnetization curve is extrapolated to zero field the net moment (μ) of the magnetic blocks is obtained. These net moments are listed in table 13 as observed moment values.

In fig. 6 the low-field magnetization curves of $Ba_2Sn_2MnFe_{10}O_{22}$ at different temperatures are shown. There is little difference between the curves of 4.2 and 77 K, but the susceptibility in the low field part of the curve has increased, indicating a less strong coupling of the magnetic blocks. At 300 K the susceptibility at low fields has increased more, and the saturation field has diminished, both indicating a further weakening of the coupling of the magnetic blocks. Because of the relatively high T_c's of the compounds the observed moment at 4.2 K can be interpreted as the highest possible ($T \approx 0$) value.

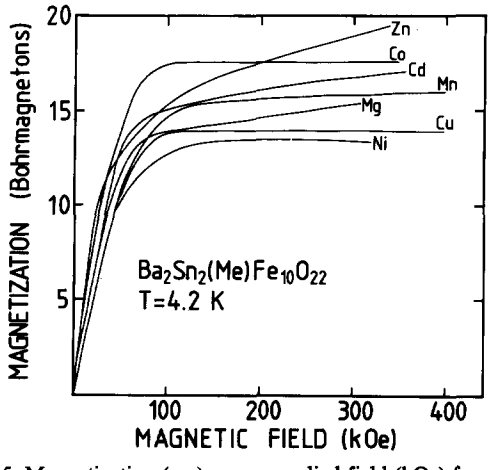

Fig. 5. Magnetization (μ_B) versus applied field (kOe) for some compounds with the QS-structure. The identity of the Me^{2+} ion is indicated in the figure.

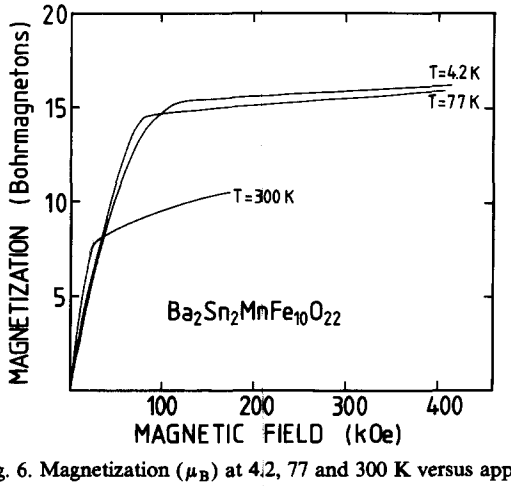

Fig. 6. Magnetization (μ_B) at 4.2, 77 and 300 K versus applied field (kOe) of $Ba_2Sn_2MnFe_{10}O_{22}$.

From table 13 can be seen that there are differences between the observed moments of the compounds at 4.2 K and the moment calculated from the data obtained from the neutron diffraction experiments.

The agreement between the calculated moments using the spin-only value and the observed moment is much better. But here also some misfits can be observed. These misfits occur at the Ni-, Co-, Zn- and Cd-compounds. For the Ni-compound this difference can be explained by the fact that the moment of Ni is higher than the spin-only value [11]. Almost the same is true for the Co-compound, in measurements of spinel-ferrites the Co-compounds have considerable higher moments than expected using the spin-only value of Co [11]. Moreover a change in the distribution of Co over the tetrahedral and octahedral sites so that Co occupies more tetrahedral sites yields also a higher moment. The differences found for the Zn- and Cd-compound can be diminished supposing Zn and Cd to occupy also octahedral sites, since the observed moment is too low. The calculated moment becomes $10\mu_B$ if Zn or Cd occupies only octahedral sites. But occupation of octahedral sites by Zn and Cd in oxyde-structures is very unusual. In quenched samples some Zn can be found at octahedral sites [22]. An explanation is that Zn and Cd occupy almost only tetrahedral sites, but that the occupation of tetrahedral sites by Zn or Cd affects the interaction between the magnetic blocks and also within the magnetic blocks. As can be observed from fig. 5, the magnetization curves of the Zn- and Cd-compound are somewhat different from the other ones, the susceptibility at low fields is higher and the saturation field is lower, which both indicates a less strong coupling between the magnetic blocks. Also at high fields the susceptibility is higher than in the other compounds, which indicates a less strong interaction within the magnetic blocks. In the M_2Y-compounds, Zn_2Y shows a different magnetic behaviour compared to the other compounds [11]. In Zn_2W ($BaZn_2Fe_{16}O_{27}$) a saturation moment of $40\mu_B$ can be expected, but a moment of $35\mu_B$ was observed, caused by canting or reversing of the moments due to Zn occupation of tetrahedral sites [23]. Attempts to prepare enough material of the Zn-compound to perform a neutron diffraction study met with no success, the Zn-compound was contaminated by other phases. Only a small quantity of the Zn-compound could be prepared in a sufficient pure grade for magnetic measurements.

A series of compounds with formula $Ba_2Sn_2Mn_{1-x}Zn_xFe_{10}O_{22}$ have been prepared for $x = 0.1$, 0.4, 0.5, 0.6, 0.7, 0.8 and 0.9 in order to investigate the Zn-compound more thoroughly. An increase of the saturation moment for low values of x was expected as is reported for compounds with formula $Zn_xMn_{1-x}Fe_2O_{44}$ [24] and also for several other spinels [25]. Indeed an increase of the saturation moment to $15.8(4)\mu_B$ was observed for the compound with $x = 0.1$. For $x = 0.4$ this moment is $15.4(4)\mu_B$, and for higher values of x a regular decrease of the moment to the value of $14.6(4)\mu_B$ for $x = 1.0$ was found. The increase of the saturation moment for low values of x is caused by the occupation of tetrahedral sites by Zn, which causes a higher net-moment of the magnetic blocks, because the moment of the octahedral sites and the tetra-hedral sites have opposite directions. For higher values of x the coupling between the magnetic blocks is affected by Zn-occupation of Tetr(2), the site that is responsible for the antiferromagnetic coupling of the magnetic blocks. This is also demonstrated by an increase of the susceptibility for fields up to 25 kOe.

An experiment with Ga-substituted compounds

Table 15
Results of the magnetic measurements of the compounds $Ba_2Sn_2MnGa_xFe_{10-x}O_{22}$ and the calculated distribution (using the spin-only value of Fe^{3+} and Mn^{2+}) of Ga^{3+} over the available tetrahedral- and octahedral sites

Compound (x)	Measured moment (μ_B)	Saturation field (kOe)	Tetrahedral sites Ga (%)	Octahedral sites Ga (%)
0	15.2 (3)	140 (10)	–	–
1	16.7 (3)	60 (10)	67	33
2	14.9 (3)	35 (10)	50	50 *
3	12.9 (3)	20 (10)	43	57
4	9.5 (4)	20 (10)	36	64
5	7.2 (4)	20 (10)	34	66

* The results of the neutron diffraction yielded 40% Ga at the tetrahedral sites.

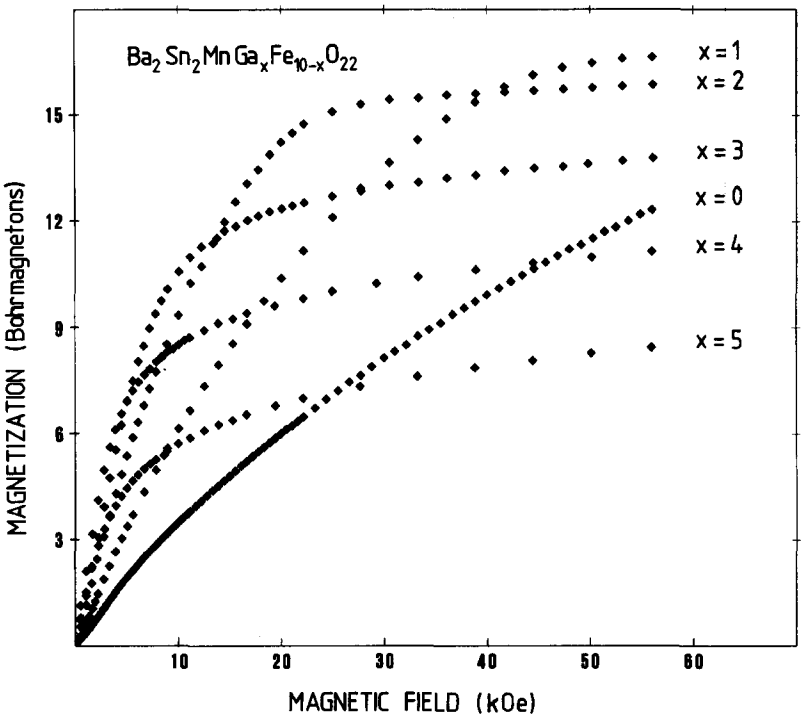

Fig. 7. Magnetization (μ_B) versus applied field (kOe) for Ga-substituted compounds of the series $Ba_2Sn_2MnGa_xFe_{10-x}O_{22}$. The value of x is indicated in the figure.

yielded simulary results. Compounds have been prepared with formula $Ba_2Sn_2MnGa_xFe_{10-x}O_{22}$ with $x = 1$, 2, 3, 4 and 5. Higher values of x yielded no pure compounds of the QS-structure. From the prepared compounds magnetization curves have been measured, the results are presented in table 15 and fig. 7. For the compound with $x = 1$ the susceptibility has strongly increased and the saturation moment has increased also compared to $Ba_2Sn_2MnFe_{10}O_{22}$. This means that Ga preferently occupies tetrahedral sites, thus increasing the net-moment of the magnetic blocks and decreasing the magnetic interaction between these blocks by occupation of Tetr(2) by Ga. This is in agreement with the results found for compounds of formula $Y_3Ga_xFe_{5-x}O_{12}$ where also a preferred occupation of tetrahedral sites by Ga was observed [26]. For $x = 2$ the saturation moment has decreased, but the susceptibility still increases. For the higher values of x an almost linear decrease of the saturation moment is observed, and the susceptibility remains almost constant for $x = 3$ and higher values of x. This means that for $x = 3$ the magnetic interaction between the blocks no longer decreases, suggesting that at least one of the two Tetr(2) sites is occupied by Ga. Both the saturation field and T_c decrease at increasing x. This indicates a decrease of the magnetic interactions between the magnetic blocks caused by occupation of Tetr(2) by Ga.

7. Conclusions

All compounds of this series have the QS-structure and form a new family of hexagonal ferrites, with magnetic properties that can be compared with the properties of $Ba_2Zn_2Fe_{12}O_{22}$ (Ferroxplana). The magnetic structure has much in common with the magnetic structure suggested for $KFe_{11}O_{17}$, described as an antiferrimagnet. As these compounds can be prepared much easier than $KFe_{11}O_{17}$, a further study of the antiferrimagnetism is now possible.

A good agreement was found between the results of the neutron diffraction and the Mössbauer spectra for the occupation of the octahedral and tetrahedral sites.

The QS-compounds show almost no remanence and the pulsed-field measurements made clear that the relaxation-time is short. These properties suggest a possible use of these compounds at high frequencies. The susceptibility for low fields can be influenced by substitutions of Zn and Ga.

Acknowledgements

We wish to thank Mr. J. Strang of the Energie-Onderzoek Centrum Nederland (E.C.N. Petten, the Netherlands) for collecting the neutron powder diffraction data, Drs. P. Schaminée of the Kamerlingh Onnes laboratory (Leiden, the Netherlands) for some measurements with the pulsed-field magnet and Drs. W.G. Haye of the Gorlaeus laboratories for some measurements with the Faraday equipment. This work is sponsored by the Leiden Materials Science Centre. The work at the Kamerlingh Onnes Laboratory is part of the research program of the Stichting voor Fundamenteel Onderzoek der Materie (Foundation for Fundamental Research on Matter) and was made possible by financial support from the Nederlandse organisatie voor Zuiver-Wetenschappelijk Onderzoek (Netherlands Organization for the Advancement of Pure Research).

References

[1] M.C. Cadée and D.J.W. IJdo, J. Solid State Chem. 36 (1981) 314.
[2] M.C. Cadée and D.J.W. IJdo, J. Solid State Chem. 40 (1981) 290.
[3] K. Weber, Acta Cryst. 23 (1967) 720.
[4] H.M. Rietveld, J. Appl. Cryst. 2 (1969) 65.
[5] F.J. van Steenwijk, Thesis, University of Leiden (1976).
[6] J.W. Arbouw, Thesis, University of Leiden (1974).
[7] H.T. Witteveen, Thesis, University of Leiden (1973).
[8] H.A. Jordaan, R. Wolf and D. de Klerk, Physica 69 (1973) 129.
[9] L. Koester and W.B. Yelon, Neutron Diffraction Newsletter (1983).
[10] R.A. Young and E. Price, J. Appl. Cryst. 15 (1982) 357.
[11] J. Smit and H.P.J. Wijn, Ferrites, Eindhoven (1959).
[12] I.I. Yamzin and J. Leciejewicz, Soviet Phys. Cryst. 15 (1970) 235.
[13] E.W. Gorter, J. Appl. Phys. 34 (1963) 1253.
[14] A.T. Howe and G.J. Dudley, J. Solid State Chem. 18 (1976) 149.
[15] Y. Abbas, F. Mostafa and M. Fayek, J. Phys. Chem. Solids 43 (1982) 973.
[16] R.F. Watson and A.J. Freeman, Acta Cryst. 14 (1961) 27.
[17] E.W. Gorter, Philips Res. Rep. 9 (1954) 403.
[18] S. Greenwald, S.J. Pickart and F.H. Granus, J. Chem. Phys. 22 (1954) 1597.
[19] Y. Abbas, F. Mostafa and M. Fayek, Acta Cryst. B39 (1983) 1.
[20] B. van Laar and D.J.W. IJdo, J. Solid State Chem. 3 (1971) 590.
[21] N.N. Greenwood and T.G. Gibb, Mössbauer Spectroscopy (Chapman and Hall, London, 1971).
[22] R. Pauthenet, Ann. Phys. 76 (1952) 710.
[23] G. Albanese, M. Carbucicchio and G. Asti, Appl. Phys. 11 (1976) 81.
[24] C. Guillaud, J. Phys. Radium 12 (1951) 1239.
[25] E.W. Gorter, Phil. Res. Rep. 9 (1954) 351.
[26] G. Amthauer, V. Gunzler, S.S. Hafner and D. Reinen, Z. Krist. 161 (1982) 167.